Research Square

Preprints are preliminary reports that have not undergone peer review.
They should not be considered conclusive, used to inform clinical practice,
or referenced by the media as validated information.

An Insert-Compatible Magnetic Actuation Platform for Dynamic Air–Liquid Interface Culture of Human Alveolar Epithelial Cells

Yu-Che Lin[1]

r08631039@ntu.edu.tw

The University of Tokyo

Shinkichi Ishikawa[3]

Japan Tobacco (Japan)

Ikuya Tanabe[3]

Japan Tobacco (Japan)

Masaki Nishikawa[2]

The University of Tokyo

Yasuyuki Sakai[2]

The University of Tokyo

Research Article

Keywords: air–liquid interface, alveolar epithelium, cyclic deformation, magnetic actuation, porous PDMS, mechanobiology

Posted Date: November 4th, 2026

DOI: https://doi.org/10.21203/rs.3.rs-11416842/v1

License: This work is licensed under a Creative Commons Attribution 4.0 International License.
Read Full License

Additional Declarations: No competing interests reported.

Abstract

Static air–liquid interface (ALI) culture reproduces apical air exposure but not breathing-associated deformation. We developed an insert-compatible magnetic actuator that cyclically deforms a porous polydimethylsiloxane (PDMS)-supported human alveolar epithelial culture while the culture plate remains lidded and free of pneumatic tubing or mechanical linkages entering the culture chamber. A polyamide-coated NdFeB magnet resting on collagen I was driven by an electromagnet beneath the plate. Short-term screening showed that coating prevented the marked MTT/LDH toxicity of an uncoated magnet. The selected 12 V, 0.2 Hz condition, operated with auxiliary convective cooling, maintained culture medium near 37°C and produced approximately 2.5 mm central displacement; geometry-based analysis estimated an annular mean strain of 7–16%. Human pulmonary alveolar epithelial cells (HPAEpiCs) were matured at ALI for 7 days and then cultured for 72 h under dynamic, static-ALI, or submerged conditions. Dynamic ALI showed higher apparent transepithelial electrical resistance than static ALI at 72 h (1780 ± 140 vs. 1634 ± 120 Ω·cm²; n = 9; p = 0.0304). At the matched 72 h endpoint, dynamic ALI also expressed the AT1-associated marker AQP5 4.3-fold higher than static ALI ($p < 0.001$), and whole-mount immunofluorescence confirmed retention of concurrent AT1- and AT2-associated features. The platform provides a compact route to add breathing-like mechanical input to an insert-based alveolar ALI workflow while preserving conventional barrier and molecular readouts.

1. Introduction

The alveolar epithelium is the final barrier for pulmonary gas exchange and a primary site of injury during acute and chronic lung disease, infection, and exposure to inhaled particles or toxicants. Chronic respiratory diseases affected an estimated 545 million people worldwide in 2017 [1], and acute respiratory distress syndrome remains common and highly lethal in intensive care units [2]. Its function depends on a thin, polarized epithelial barrier that is continuously deformed by breathing [3, 4]. Alveolar type 1 (AT1) cells provide the broad gas-exchange surface, whereas alveolar type 2 (AT2) cells secrete surfactant and serve as progenitors during homeostasis and repair [5, 6]. Consequently, physiologically relevant in vitro models should reproduce not only epithelial identity and barrier function but also the air-facing and mechanical environment of the distal lung.

Cell source remains a major limitation in alveolar modeling. Primary human AT1 cells are fragile and difficult to maintain, while isolated AT2 cells rapidly lose mature features in conventional two-dimensional culture. Immortalized lines are experimentally convenient but do not reproduce the full barrier and lineage programs of primary alveolar epithelium. Recent approaches therefore use expandable primary/progenitor-like cells, induced pluripotent stem cell (iPSC)-derived AT2 and AT1 cells, and alveolar organoids, often followed by transfer to an air–liquid interface (ALI) to promote epithelial polarization and maturation [7–11]. Our previous HPAEpiC study established an insert-based ALI condition that maintained a mixed AT1/AT2-associated phenotype together with a high-resistance epithelial barrier [10], providing a practical biological basis for adding breathing-related mechanical stimulation.

Several established systems can impose cyclic deformation on cultured cells [12]. Commercial platforms such as the Flexcell FX-6000T use vacuum/air pressure to deform dedicated flexible-bottom culture plates [13], whereas STREX systems apply motor-driven stretch to dedicated silicone chambers [14]. Breathing lung-on-chip platforms provide more lung-specific architectures: early microfluidic devices reproduced an alveolar–capillary interface and cyclic deformation [15], and the AlveoliX-derived breathing chip architecture enables multiwell operation and transepithelial electrical resistance (TEER) measurement [16, 17]. Pressure-actuated MALI/CIVIC bioreactors further combine ALI culture with membrane stretch and aerosol exposure [18, 19]. These systems provide valuable control of deformation, flow, or multicellular interfaces, but generally depend on specialized flexible chambers/chips and pneumatic or mechanical actuation hardware. For routine insert culture, a magnetic approach offers a different engineering trade-off: force can be transmitted across a closed, lidded culture plate without pneumatic tubing or a mechanical linkage entering the culture chamber, potentially reducing handling and contamination pathways while retaining conventional insert-based sampling.

Magnetic actuation has recently been applied to lung epithelial mechanobiology. Wei et al. developed magnetoactive kirigami-inspired hammocks in which human small-airway epithelial cells responded to dynamic magnetic stimulation with increased proliferation and cytoskeletal reinforcement [20]. That approach demonstrated the feasibility of magnetic lung-cell stimulation, but it did not address an alveolar ALI insert workflow with barrier measurements and routine RNA/imaging recovery. We therefore developed an insert-compatible magnetic platform around a porous PDMS membrane and a coated permanent magnet positioned above an electromagnet. Because resistive heating is an obvious concern for any electromagnet operated for prolonged cell culture, thermal characterization and cooling were treated as primary design requirements rather than secondary engineering checks. The study asks whether this configuration can deliver reproducible cyclic deformation under thermally and biologically compatible conditions and whether an established HPAEpiC ALI barrier remains functional and phenotypically recoverable during 72 h of dynamic culture.

2. Materials and Methods

2.1. Porous PDMS membrane preparation and surface functionalization

Porous PDMS membranes were fabricated in-house on a micropillar mold provided by Prof. Kimura's laboratory (Tokai University, Japan). The pillars defined through-pores of 100 μm diameter arranged at a 200 μm pitch, giving a porosity of approximately 19%. The mold was first spin-coated with a sacrificial poly(vinyl alcohol) layer (10 mg/mL; 4000 rpm, 60 s) and then with 10 g of PDMS (10:1 base:curing agent; 2000 rpm, 20 s, a spin speed optimized in this study from the initial 1000–1500 rpm protocol), which was cured overnight. The insert was placed on the cured PDMS film, the PVA layer was dissolved in water for 1 day, and the membrane was peeled from the mold. Through-pores were confirmed by transmission of colored water, and thickness was measured with a measuring microscope

(approximately 70 μm). Membranes were then activated with oxygen plasma and treated sequentially with 6.7% (3-aminopropyl)triethoxysilane (APTES) for 20 min and 2.5% glutaraldehyde for 1 h, with washing between steps, before collagen I coating, so that collagen was covalently immobilized rather than adsorbed [21–24].

2.2. Magnet coating and short-term cytocompatibility

An approximately 8.2-mm-diameter NdFeB permanent magnet was protected with a polyamide coating before biological use. Short-term coating cytocompatibility was evaluated after 24 h using MTT metabolic-viability and LDH-release assays in normal culture, cultures exposed to a polyamide-coated magnet, and cultures exposed to an uncoated Nd magnet (n = 3 per group). MTT values were normalized to normal culture and LDH release was expressed relative to assay controls. Group differences were analyzed by one-way ANOVA followed by Tukey HSD.

2.3. Magnetic actuation platform, deformation analysis, and thermal control

The six-position platform aligned each insert above an electromagnet while the polyamide-coated permanent magnet rested directly on the epithelial cell layer on the apical surface of a 3 mg/mL collagen I gel supported by the porous PDMS membrane (Fig. 1). The culture plate remained lidded during actuation. A 0–5 V triangular control waveform at 0.2 Hz drove the controller, and the board was powered by a 12 V DC supply for biological experiments. The downward motion of the magnet–gel–membrane assembly was quantified from side-view video using the far membrane edge as a fixed reference.

A geometry-based sensitivity analysis was used to describe the expected spatial deformation without assigning a uniform cellular strain. The nominal culture area (452.4 mm^2) was represented by a radius of approximately 12.0 mm; after excluding the outer approximately 1 mm bonded rim, the free membrane radius was set to R = 11.0 mm. The rigid magnet-contact radius was Rm = 4.10 mm. Outside the contact region, the displacement profile was approximated as $w(r) = h \ln(R/r)/\ln(R/Rm)$, and meridional geometric strain was estimated as $\varepsilon = \sqrt{[1 + (dw/dr)^2]} - 1$ for h = 2.5–4.0 mm.

Thermal characterization was performed at 12, 16, and 21 V with and without an auxiliary fan, and coil-surface and culture-medium temperatures were followed for 240 min; medium temperature was treated as the biologically relevant endpoint. All experiments were conducted in a large-capacity CO_2 incubator (MCO-80IC-PJ; PHC Corporation, Tokyo, Japan; interior volume 851 L; heater output 570 W; heater with forced-air circulation) set to 37°C. The auxiliary fan was a small unbranded handheld fan placed inside the incubator 3 cm from the device, outside the lidded culture plate, and operated continuously at its lowest setting during dynamic culture. Fan speed, air velocity, and volumetric flow rate were not instrument-calibrated. The measured supply current for the tested electromagnet at 12 V was approximately 0.04 A, corresponding to an electrical input of approximately 0.48 W. Assuming comparable current in six simultaneously operated channels, the aggregate electrical input would be

approximately 2.9 W; this aggregate value was not directly measured, and these values represent electrical input rather than calorimetric heat generation. Coil-surface temperature was recorded with a handheld infrared thermal camera (ZOHIKO) at a fixed point on the coil housing, and culture-medium temperature was measured with the same camera immediately after removing the plate lid.

2.4. HPAEpiC culture and dynamic experimental groups

Commercial human pulmonary alveolar epithelial cells (HPAEpiCs; ScienCell Research Laboratories, Carlsbad, CA, USA) were expanded in Alveolar Epithelial Cell Medium using the small-molecule-supported workflow established previously [10]. Cells were seeded onto collagen-functionalized porous PDMS at approximately 4×10^4 cells/cm², allowed to attach under submerged conditions, and then transferred to ALI by removing apical medium. After 7 days of ALI maturation, inserts entered a 72 h experimental phase: dynamic ALI at 0.2 Hz under the selected 12 V condition with continuous fan cooling, static ALI without actuation, or submerged culture. The 72 h interval was selected as a sustained short-term mechanostimulation window after establishment of the mature ALI barrier; at 0.2 Hz it corresponds to approximately 5.2×10^4 loading cycles, allowing barrier and molecular responses to be assessed without extending the study to longer-term remodeling. Independent inserts were treated as biological replicates.

2.5. TEER, RT-qPCR, and immunofluorescence readouts

TEER was measured during ALI maturation (days 0, 3, 5, and 7) and after 24, 48, and 72 h of the experimental phase using an EVOM3 epithelial volt/ohm meter with STX2 chopstick electrodes (World Precision Instruments, Sarasota, FL, USA). Before measurement, the apical compartment was temporarily rehydrated with pre-warmed medium; blank-corrected resistance was multiplied by nominal culture area and is reported as apparent TEER because the integrated magnet/collagen assembly can alter current paths [25]. The final TEER dataset comprised nine independent inserts per condition.

For RT-qPCR, RNA extraction, reverse transcription, and SYBR Green analysis followed the established HPAEpiC workflow [10]. SFTPB and SFTPC were used as AT2-associated markers, AQP5 and PDPN as AT1-associated markers, and GAPDH as the reference gene. Relative expression was calculated by the $2^{-\Delta\Delta Cq}$ method [26]. Primer sequences are listed in Online Resource 1 (Table S1). Dynamic samples were collected at 24, 48, and 72 h, whereas the static-ALI and submerged molecular controls were collected at the matched 72 h endpoint.

Whole-mount immunofluorescence combined AQP5 and PDPN with either SP-B or ABCA3; the two AT2-associated proteins were assessed in separate staining sets because both primary antibodies were raised in rabbit. Confocal panels were reconstructed from original OIR files using matched physical field dimensions and 20 μm scale bars. Because acquisition settings were not fully harmonized across all files, fluorescence was interpreted qualitatively for localization and morphology rather than as an intensity-based quantitative endpoint.

2.6. Statistical analysis

The pre-specified 72 h dynamic-versus-static TEER comparison used a two-sided independent-samples t test. For RT-qPCR, the three groups sampled at 72 h (submerged, static ALI, and dynamic ALI) were compared by one-way ANOVA followed by Tukey HSD on replicate-level ΔCq values; dynamic samples at 24 and 48 h are shown descriptively in Online Resource 1 (Fig. S1). Magnet cytocompatibility used one-way ANOVA followed by Tukey HSD. Data are shown as mean ± SD unless stated otherwise.

3. Results and Discussion

3.1. A selected porous PDMS membrane supported insert-based ALI culture

The final membrane was 10:1 PDMS spin-coated at 2000 rpm (approximately 70 μm thick; approximately 19% porosity; Fig. 2). Preliminary mechanical screening was used only to select a membrane that tolerated localized magnetic loading while remaining sufficiently deformable for cyclic operation. Plasma-assisted APTES/glutaraldehyde functionalization followed by collagen I supported epithelial attachment, whereas untreated PDMS did not provide stable coverage. Representative phase-contrast imaging confirmed that HPAEpiCs attached and spread on the collagen-functionalized porous PDMS membrane, forming coverage between the regularly spaced through-pores (Fig. 2).

3.2. Polyamide coating resolved the dominant short-term magnet cytotoxicity

The uncoated Nd magnet was strongly cytotoxic after 24 h, whereas the polyamide-coated magnet was indistinguishable from normal culture in both assays (Fig. 3). MTT viability was 100.0% in normal culture, 100.3% with the coated magnet ($p = 0.99$), and 31.3% with the uncoated magnet ($p < 0.001$ versus both other groups). LDH cytotoxicity was 0.0%, − 3.1%, and 61.8%, respectively; the coated condition did not differ from normal culture ($p = 0.52$), whereas the uncoated magnet was higher than both ($p < 0.001$). The assay establishes short-term compatibility; long-term coating durability and ion leaching remain to be tested.

3.3. Magnetic actuation generated localized deformation within a thermally controlled operating window

Side-view imaging confirmed approximately 2.5 mm downward displacement of the membrane lowest point in the representative recording, while the far edge remained nearly stationary (Fig. 4). The motion therefore cannot be represented by a single whole-well strain value. The geometry-based analysis predicted the highest meridional strain near the magnet edge and radial decay toward the insert boundary; across $h = 2.5–4.0$ mm, the annular mean estimate was 7–16% and the corresponding annular surface-area increase was 12–31% (Fig. 5). These values define a plausible deformation envelope rather

than a direct cellular strain map; direct fiducial tracking or validated finite-element analysis would be required for spatial mechanobiology claims.

Electromagnet heating was the principal engineering safety constraint. Without the fan, the medium plateau exceeded 37°C at every voltage tested (41.5, 43.7, and 46.4°C at 12, 16, and 21 V; Fig. 6). Fan-assisted cooling lowered the medium plateau by 1.3–4.7°C; only 12 V with the fan kept the medium at 37.1 ± 0.2°C, within the predefined acceptable range (≤ 38°C), whereas 16 and 21 V with the fan reached 39.0 and 45.1°C. To place this electrical load in context, the measured input for the tested electromagnet at 12 V was approximately 0.48 W; assuming comparable current across six simultaneously operated channels, the corresponding aggregate input would be approximately 2.9 W. These values are less than 0.1% and about 0.5%, respectively, of the incubator's rated 570 W heater output, but the comparison is only contextual because the heater rating does not represent active cooling capacity. Despite the relatively small electrical load, the medium still reached 41.5°C without the fan, indicating that local heat accumulation in the confined space beneath the culture plate, rather than total incubator heating capacity, governed the culture temperature. Consistent with this interpretation, the fan lowered the medium plateau much more than the coil-surface temperature at 12 V (4.4°C versus 0.3°C), indicating that it acted mainly by improving local convective heat removal beneath the plate. The fan is therefore an essential component of the operating configuration, and 12 V with continuous fan cooling was used for all biological experiments. Because this thermal balance depends on local airflow, it should be re-verified when the platform is used in a different incubator or when several boards are operated simultaneously.

3.4. Dynamic ALI culture preserved barrier function and produced a higher endpoint TEER

Apparent TEER increased progressively during the 7-day ALI maturation phase, from 230 ± 40 Ω·cm² on day 0 to 1,262 ± 90 Ω·cm² on day 7 (n = 9), establishing a high-resistance baseline before mechanical stimulation (Fig. 7a). During the subsequent 72 h comparison, the order of mean TEER was submerged < static ALI < dynamic ALI at each measured time point (Fig. 7b). At 72 h, dynamic ALI reached 1,780 ± 140 Ω·cm² versus 1,634 ± 120 Ω·cm² in static ALI, a mean difference of 146 Ω·cm² (8.9%; $t(16) = 2.375$, $p = 0.0304$; 95% CI, 16–276; Cohen's $d = 1.12$).

The result shows that 72 h of magnetic cyclic deformation did not compromise the mature epithelial barrier and was associated with a modest but statistically supported increase in the whole-insert electrical readout. Biologically, this is important because the cells were mechanically stimulated only after a high-resistance ALI barrier had already formed; the higher endpoint TEER therefore indicates that the mature epithelium remained responsive to a breathing-related mechanical cue rather than merely tolerating device operation. Cyclic deformation can either reinforce or disrupt junctional organization depending on amplitude and exposure context [27–33]; therefore, the present result should be interpreted as a system-level barrier response rather than proof of uniform junctional strengthening at every position on the membrane.

3.5. Dynamic ALI increased selected alveolar epithelial markers at the matched 72 h endpoint

RT-qPCR detected concurrent AT2-associated SFTPB/SFTPC and AT1-associated AQP5/PDPN expression in the ALI cultures (Fig. 8). At the matched 72 h endpoint, when all three groups were sampled, dynamic ALI expressed AQP5 at 19.5 ± 4.9 versus 4.5 ± 0.4 in static ALI (relative to submerged culture; 4.3-fold; $p < 0.001$), SFTPB at 8.9 ± 2.3 versus 3.4 ± 0.6 (2.6-fold; $p = 0.003$), and PDPN at 5.6 ± 0.2 versus 3.3 ± 0.5 (1.7-fold; $p = 0.008$), whereas SFTPC did not differ ($p = 0.82$). Thus, the transcriptional response was selective rather than a uniform increase in all alveolar markers.

The biological significance of this pattern is that repeated mechanical input altered the phenotype-associated program of an already mature alveolar epithelial barrier, rather than simply preserving cell survival. The particularly strong increase in AQP5 together with higher PDPN is consistent with an AT1-associated adaptation relevant to the thin gas-exchange surface, whereas the concurrent increase in SFTPB indicates that AT2-associated characteristics were not lost. The unchanged SFTPC further argues against a uniform lineage conversion. Previous studies have reported divergent alveolar epithelial responses to stretch, including AT1-associated adaptation, maintenance or enhancement of surfactant programs, and injury-associated responses depending on cell source, developmental state, strain magnitude, waveform, and duration [31–35]. Accordingly, the present result is best interpreted as selective mechanobiological modulation of a mixed alveolar phenotype. The 24–48–72 h dynamic-only series is provided in Online Resource 1 (Fig. S1); because static-ALI and submerged controls were not collected at 24 and 48 h, this series is descriptive and is not used to infer an actuation-specific temporal trajectory.

Whole-mount immunofluorescence confirmed that both AT1- and AT2-associated proteins remained detectable after dynamic culture (Fig. 9). AQP5 signal was broadly distributed, PDPN was weaker or discontinuous, and SP-B/ABCA3 showed heterogeneous cell-associated localization. In the SP-B staining set, representative dynamic fields showed visually more prominent SP-B- and AQP5-associated signal than the corresponding static field; however, acquisition settings were not fully harmonized, so no quantitative fluorescence comparison is claimed. The imaging therefore provides protein-level support that dynamic culture preserved concurrent AT1- and AT2-associated features, complementing the barrier and transcript data without being used as independent evidence of lineage conversion.

Taken together, the biological data show that the magnetic platform did more than maintain cell viability during 72 h of actuation. Dynamic ALI preserved a high-resistance epithelial barrier, produced a significantly higher endpoint apparent TEER than static ALI, and selectively increased AQP5, PDPN, and SFTPB expression at the matched 72 h endpoint. The combination of a stronger barrier readout with an AT1-associated shift while retaining AT2-associated features supports the interpretation that breathing-like mechanical input acts as a regulatory cue for alveolar epithelial homeostasis and phenotype. This conclusion is intentionally restricted to the matched 72 h epithelial comparison; additional 24 and 48 h static/submerged controls would be required only for claims about the temporal trajectory of actuation-

specific transcriptional responses. Quantitative imaging under harmonized acquisition settings and vertical histology remain complementary validation. Longer-duration studies or addition of stromal/endothelial compartments would address distinct questions of chronic remodeling and epithelial–mesenchymal interaction rather than a missing control for the present short-term platform study.

4. Conclusions

We established a magnetic actuation strategy that adds breathing-like cyclic deformation to a conventional insert-based alveolar ALI workflow without pneumatic tubing or mechanical linkages entering the culture chamber. Polyamide coating eliminated the strong short-term toxicity observed with an uncoated Nd magnet, and active convective cooling defined a thermally compatible 12 V, 0.2 Hz operating condition. Under this condition, the membrane exhibited approximately 2.5 mm central displacement and HPAEpiCs maintained a high-resistance barrier during 72 h of dynamic culture. Dynamic ALI showed higher apparent TEER than static ALI at 72 h and selectively increased the AT1-associated markers AQP5 and PDPN together with the AT2-associated marker SFTPB, while SFTPC remained unchanged. These findings indicate that sustained mechanical input is not merely tolerated by the mature ALI epithelium but can modulate barrier function and selected alveolar phenotype-associated programs. The principal contribution is therefore an insert-compatible platform that couples conventional ALI culture with a biologically active mechanical cue while retaining standard barrier, molecular, and imaging readouts. Vertical histology and direct local-strain measurements will further refine the structural and mechanical interpretation.

Declarations

Competing interests

S.I. and I.T. are employees of Japan Tobacco Inc. The other authors declare no relevant financial or non-financial interests.

Ethics approval

Not applicable. The study used commercially available human pulmonary alveolar epithelial cells and did not recruit human participants or use animals.

Consent to participate

Not applicable.

Consent for publication

Not applicable.

Funding

This study was funded by Japan Tobacco Inc.

Author Contribution

Conceptualization, Y.-C.L. and Y.S.; methodology, Y.-C.L.; formal analysis, Y.-C.L.; investigation, Y.-C.L.; resources, S.I., M.N. and Y.S.; visualization, Y.-C.L.; writing—original draft, Y.-C.L.; writing—review and editing, S.I., I.T., M.N. and Y.S.; supervision, M.N. and Y.S. All authors read and approved the final manuscript.

Acknowledgement

AcknowledgmentsThe authors would like to express their sincere gratitude to Prof. Hiroshi Kimura, Kenta Shimba, and Jin Hong Yap of Tokai University for providing the micropillar mold and technical guidance on porous PDMS membrane fabrication. We also thank Prof. Ito and N. Inagaki for providing access to their laboratory's mechanical testing equipment and assistance with Young's modulus measurements of the PDMS membranes. Their generous support and technical assistance are gratefully acknowledged.

Data availability

The datasets supporting the findings of this study are available from the corresponding author upon reasonable request, subject to institutional and collaborative restrictions.

References

1. GBD Chronic Respiratory Disease Collaborators, Prevalence and attributable health burden of chronic respiratory diseases, 1990–2017: a systematic analysis for the Global Burden of Disease Study 2017. Lancet Respir Med. **8**, 585–596 (2020). https://doi.org/10.1016/S2213-2600(20)30105-3
2. G. Bellani, J.G. Laffey, T. Pham et al., Epidemiology, patterns of care, and mortality for patients with acute respiratory distress syndrome in intensive care units in 50 countries. JAMA **315**, 788–800 (2016). https://doi.org/10.1001/jama.2016.0291

3. D.J. Tschumperlin, S.S. Margulies, Alveolar epithelial surface area-volume relationship in isolated rat lungs. J. Appl. Physiol. **86**, 2026–2033 (1999). https://doi.org/10.1152/jappl.1999.86.6.2026
4. Y. Cui, F.M. Hameed, B. Yang et al., Cyclic stretching of soft substrates induces spreading and growth. Nat. Commun. **6**, 6333 (2015). https://doi.org/10.1038/ncomms7333
5. C.E. Barkauskas, M.J. Cronce, C.R. Rackley et al., Type 2 alveolar cells are stem cells in adult lung. J. Clin. Invest. **123**, 3025–3036 (2013). https://doi.org/10.1172/JCI68782
6. A.N. Nabhan, D.G. Brownfield, P.B. Harbury, M.A. Krasnow, T.J. Desai, Single-cell Wnt signaling niches maintain stemness of alveolar type 2 cells. Science. **359**, 1118–1123 (2018). https://doi.org/10.1126/science.aam6603
7. I. Tanabe, K. Ishimori, S. Ishikawa, Development of an in vitro human alveolar epithelial air-liquid-interface model using a small molecule inhibitor cocktail. BMC Mol. Cell. Biol. **25**, 9 (2024). https://doi.org/10.1186/s12860-024-00507-7
8. I. Tanabe, S. Ishikawa, Comprehensive characterization of human alveolar epithelial cells cultured for 28 days at the air-liquid interface. Sci. Rep. **15**, 22995 (2025). https://doi.org/10.1038/s41598-025-07219-8
9. A. Jacob, M. Morley, F. Hawkins et al., Differentiation of human pluripotent stem cells into functional lung alveolar epithelial cells. Cell. Stem Cell. **21**, 472–488e10 (2017). https://doi.org/10.1016/j.stem.2017.08.014
10. Y.-C. Lin, M. Igarashi, Y. Sakai, M. Nishikawa, S. Ishikawa, I. Tanabe, Wnt-dependent modulation of alveolar epithelial phenotypes and barrier function in human progenitor-like cells. Biochem. Biophys. Res. Commun. **807**, 153384 (2026). https://doi.org/10.1016/j.bbrc.2026.153384
11. van S. Riet, D.K. Ninaber, H.M.M. Mikkers et al., In vitro modelling of alveolar repair at the air-liquid interface using alveolar epithelial cells derived from human induced pluripotent stem cells. Sci. Rep. **10**, 5499 (2020). https://doi.org/10.1038/s41598-020-62226-1
12. C. Moraes, J.-H. Chen, Y. Sun, C.A. Simmons, Microfabricated arrays for high-throughput screening of cellular response to cyclic substrate deformation. Lab. Chip. **10**, 227–234 (2010). https://doi.org/10.1039/B914460A
13. A.J. Banes, J. Gilbert, D. Taylor, O. Monbureau, A new vacuum-operated stress-providing instrument that applies static or variable duration cyclic tension or compression to cells in vitro. J. Cell. Sci. **75**, 35–42 (1985)
14. K. Naruse, T. Yamada, M. Sokabe, Involvement of SA channels in orienting response of cultured endothelial cells to cyclic stretch. Am. J. Physiol. **274**, H1532–H1538 (1998)
15. D. Huh, B.D. Matthews, A. Mammoto, M. Montoya-Zavala, H.Y. Hsin, D.E. Ingber, Reconstituting organ-level lung functions on a chip. Science. **328**, 1662–1668 (2010). https://doi.org/10.1126/science.1188302
16. J.D. Stucki, N. Hobi, A. Galimov et al., Medium throughput breathing human primary cell alveolus-on-chip model. Sci. Rep. **8**, 14359 (2018). https://doi.org/10.1038/s41598-018-32523-x

17. M. Felder, B. Trueeb, A.O. Stucki et al., Impaired wound healing of alveolar lung epithelial cells in a breathing lung-on-a-chip. Front. Bioeng. Biotechnol. **7**, 3 (2019). https://doi.org/10.3389/fbioe.2019.00003
18. D. Cei, A. Doryab, A.-G. Lenz et al., Development of a dynamic in vitro stretch model of the alveolar interface with aerosol delivery. Biotechnol. Bioeng. **118**, 690–702 (2021). https://doi.org/10.1002/bit.27600
19. A. Doryab, M.B. Taskin, P. Stahlhut et al., A bioinspired in vitro lung model to study particokinetics of nano-/microparticles under cyclic stretch and air-liquid interface conditions. Front. Bioeng. Biotechnol. **9**, 616830 (2021). https://doi.org/10.3389/fbioe.2021.616830
20. K. Wei, A. Roy, S. Ejike et al., Magnetoactive, kirigami-inspired hammocks to probe lung epithelial cell function. Cell. Mol. Bioeng. **17**, 317–327 (2024). https://doi.org/10.1007/s12195-024-00808-z
21. P.-J. Wipff, H. Majd, C. Acharya, L. Buscemi, J.-J. Meister, B. Hinz, The covalent attachment of adhesion molecules to silicone membranes for cell stretching applications. Biomaterials. **30**, 1781–1789 (2009). https://doi.org/10.1016/j.biomaterials.2008.12.022
22. J.N. Lee, X. Jiang, D. Ryan, G.M. Whitesides, Compatibility of mammalian cells on surfaces of poly(dimethylsiloxane). Langmuir. **20**, 11684–11691 (2004). https://doi.org/10.1021/la048562+
23. S. Kuddannaya, Y.J. Chuah, M.H.A. Lee, N.V. Menon, Y. Kang, Y. Zhang, Surface chemical modification of poly(dimethylsiloxane) for the enhanced adhesion and proliferation of mesenchymal stem cells. ACS Appl. Mater. Interfaces. **5**, 9777–9784 (2013). https://doi.org/10.1021/am402903e
24. K. Mori, K. Kataoka, Y. Akiyama, T. Asahi, Covalent immobilization of collagen type I to a polydimethylsiloxane surface for preventing cell detachment by retaining collagen molecules under uniaxial cyclic mechanical stretching stress. Biomacromolecules. **24**, 5035–5045 (2023). https://doi.org/10.1021/acs.biomac.3c00669
25. B. Srinivasan, A.R. Kolli, M.B. Esch, H.E. Abaci, M.L. Shuler, J.J. Hickman, TEER measurement techniques for in vitro barrier model systems. J. Lab. Autom. **20**, 107–126 (2015). https://doi.org/10.1177/2211068214561025
26. K.J. Livak, T.D. Schmittgen, Analysis of relative gene expression data using real-time quantitative PCR and the 2^−ΔΔCT method. Methods. **25**, 402–408 (2001). https://doi.org/10.1006/meth.2001.1262
27. K.J. Jr Cavanaugh, J. Oswari, S.S. Margulies, Role of stretch on tight junction structure in alveolar epithelial cells. Am. J. Respir Cell. Mol. Biol. **25**, 584–591 (2001). https://doi.org/10.1165/ajrcmb.25.5.4486
28. D.J. Tschumperlin, S.S. Margulies, Equibiaxial deformation-induced injury of alveolar epithelial cells in vitro. Am. J. Physiol. Lung Cell. Mol. Physiol. **275**, L1173–L1183 (1998). https://doi.org/10.1152/ajplung.1998.275.6.L1173
29. L.P. Desai, K.E. Chapman, C.M. Waters, Mechanical stretch decreases migration of alveolar epithelial cells through mechanisms involving Rac1 and Tiam1. Am. J. Physiol. Lung Cell. Mol. Physiol. **295**, L958–L965 (2008). https://doi.org/10.1152/ajplung.90218.2008

30. M.J. Song, N. Davidovich, G.G. Lawrence, S.S. Margulies, Superoxide mediates tight junction complex dissociation in cyclically stretched lung slices. J. Biomech. **49**, 1330–1335 (2016). https://doi.org/10.1016/j.jbiomech.2015.10.032
31. J. Sanchez-Esteban, L.A. Cicchiello, Y. Wang, S.-W. Tsai, L.K. Williams, J.S. Torday, L.P. Rubin, Mechanical stretch promotes alveolar epithelial type II cell differentiation. J. Appl. Physiol. **91**, 589–595 (2001). https://doi.org/10.1152/jappl.2001.91.2.589
32. C.D. Foster, L.S. Varghese, L.W. Gonzales, S.S. Margulies, S.H. Guttentag, The Rho pathway mediates transition to an alveolar type I cell phenotype during static stretch of alveolar type II cells. Pediatr. Res. **67**, 585–590 (2010). https://doi.org/10.1203/PDR.0b013e3181dbc708
33. H. Ye, Q. Zhan, Y. Ren, X. Liu, C. Yang, C. Wang, Cyclic deformation-induced injury and differentiation of rat alveolar epithelial type II cells. Respir Physiol. Neurobiol. **180**, 237–246 (2012). https://doi.org/10.1016/j.resp.2011.11.011
34. K. Shiraishi et al., Biophysical forces mediated by respiration maintain lung alveolar epithelial cell fate. Cell. **186**, 1478–1492e15 (2023). https://doi.org/10.1016/j.cell.2023.02.010
35. K.L. Leiby et al., Rational engineering of a human alveolar lung-on-chip model with physiologic function and cellular plasticity. npj Regen Med. **8**, 22 (2023). https://doi.org/10.1038/s41536-023-00295-2

Figures

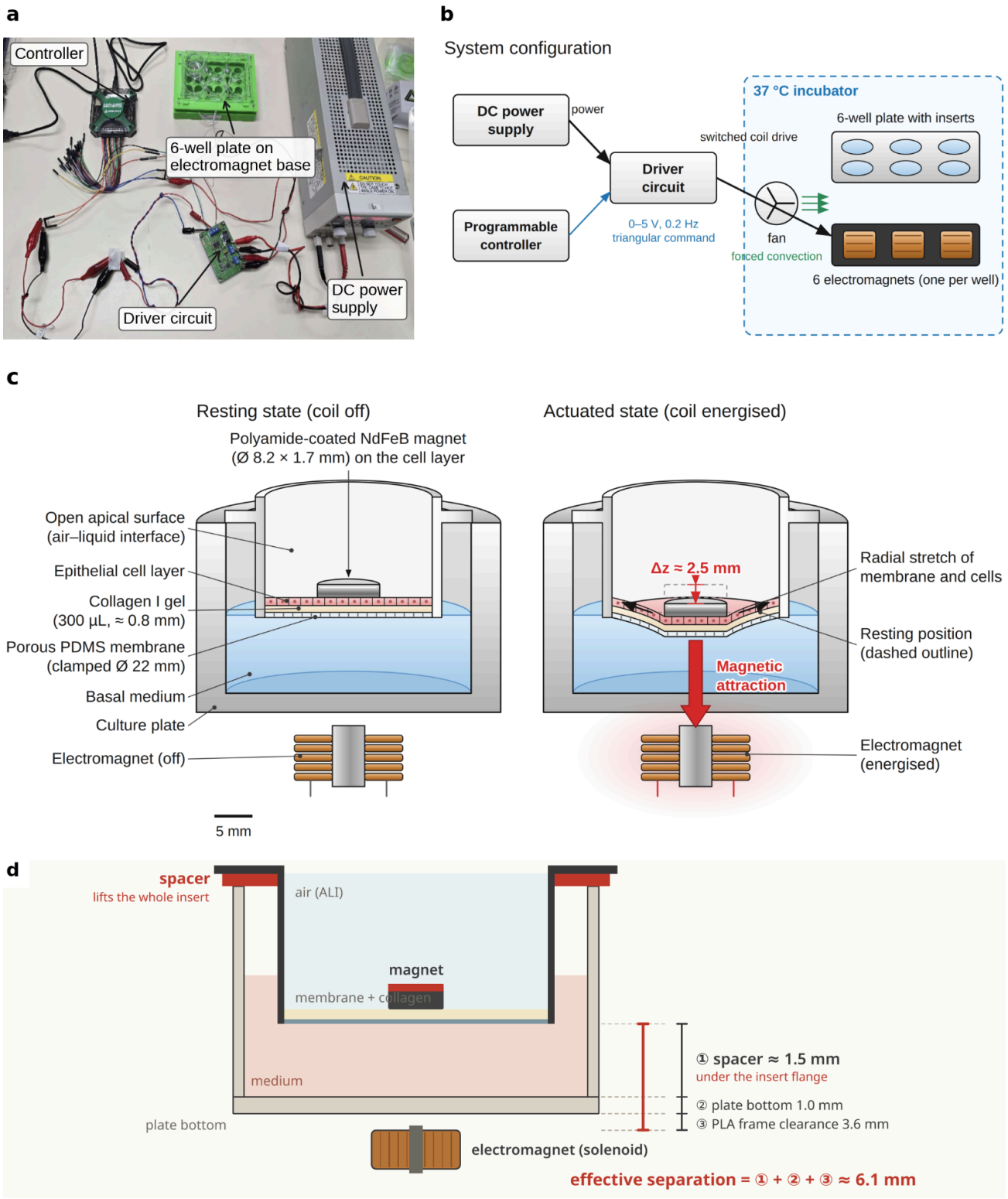


Figure 1

Magnetic actuation platform and working gap geometry. (a) Hardware, shown on the bench before placement in the incubator: programmable controller, driver circuit, DC power supply, and the 6-well plate on the electromagnet base. (b) System configuration: a programmable controller supplies a 0–5 V, 0.2 Hz triangular command to a driver circuit that drives six electromagnets, one beneath each well of the lidded 6-well plate, inside a 37 °C incubator with an auxiliary fan. (c) Cross-section of an insert at rest

and during actuation. A polyamide-coated NdFeB magnet (Ø 8.2 × 1.7 mm) is positioned on the apical side of the collagen-supported epithelial culture over the porous PDMS membrane; energizing the electromagnet pulls the central membrane region downward by approximately 2.5 mm. (d) Working gap geometry. A spacer (~1.5 mm) beneath the insert flange raises the whole insert; together with the plate bottom (~1.0 mm) and PLA-frame clearance (~3.6 mm), the effective magnet–coil separation is approximately 6.1 mm. The spacer is not located beneath the membrane. Schematics are not to scale unless indicated; scale bar in (c), 5 mm

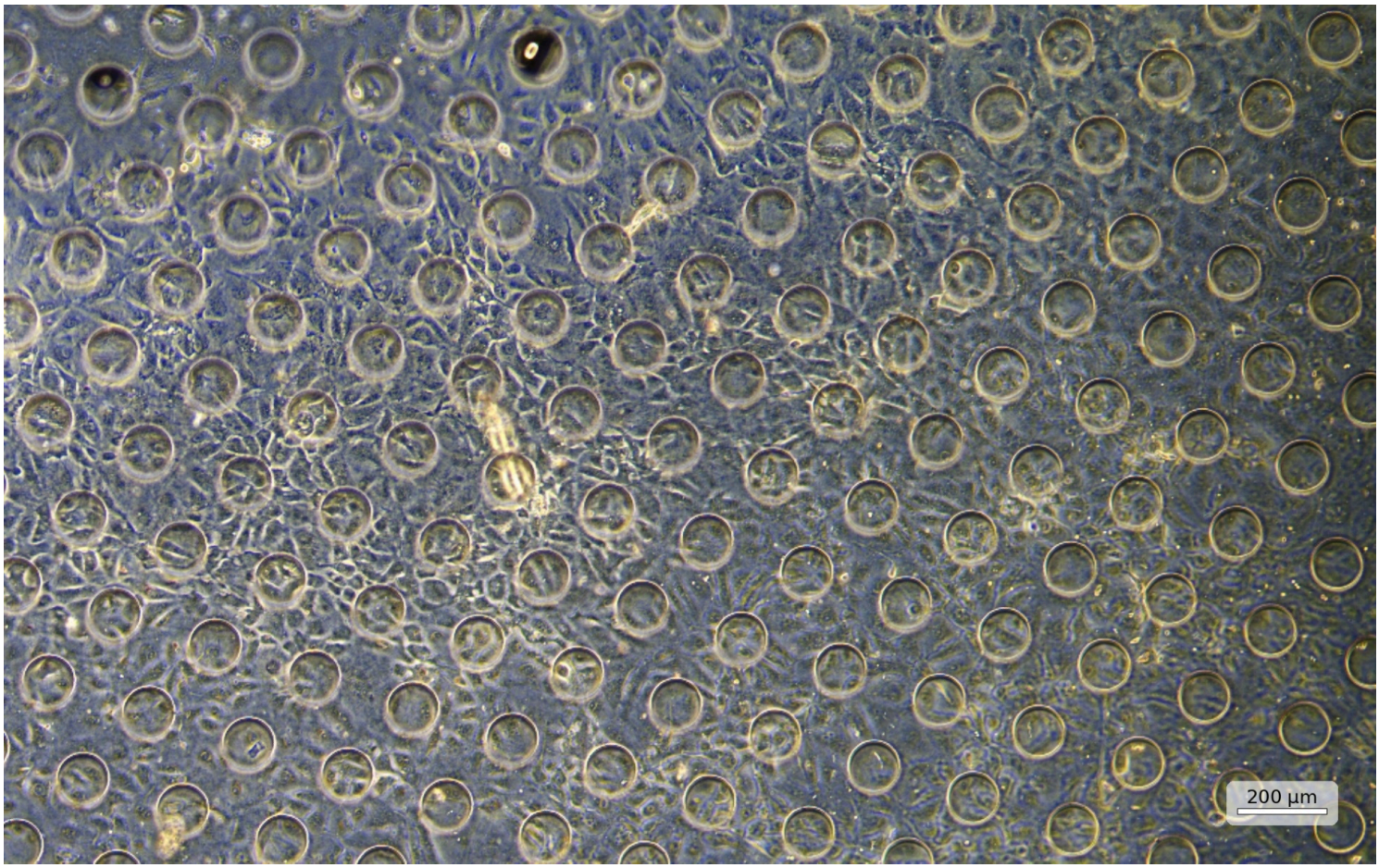


Figure 2

Representative phase-contrast image of HPAEpiCs cultured on the collagen-coated porous PDMS membrane. Regular through-pores (100 µm diameter, 200 µm pitch; porosity ~19%) are visible beneath the epithelial layer, showing cell attachment and spreading on the membrane surface between pores. Scale bar, 200 µm, calibrated from the pore pitch

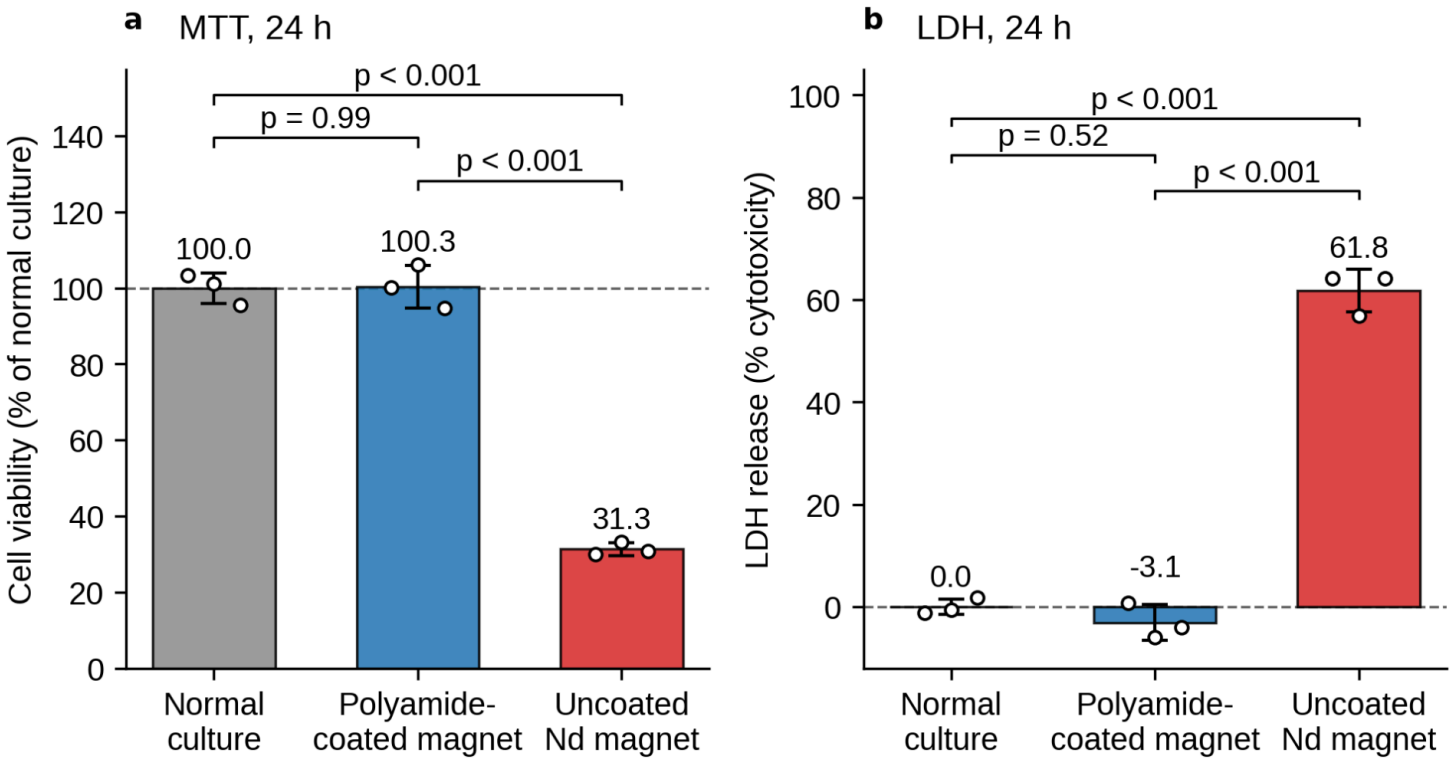


Figure 3

Short-term cytocompatibility of polyamide-coated and uncoated neodymium magnets. (a) MTT viability after 24 h, normalized to normal culture. (b) LDH release expressed as percent cytotoxicity. Bars show mean ± SD and circles indicate independent replicates (n = 3 per group). One-way ANOVA with Tukey HSD; exact p values are shown

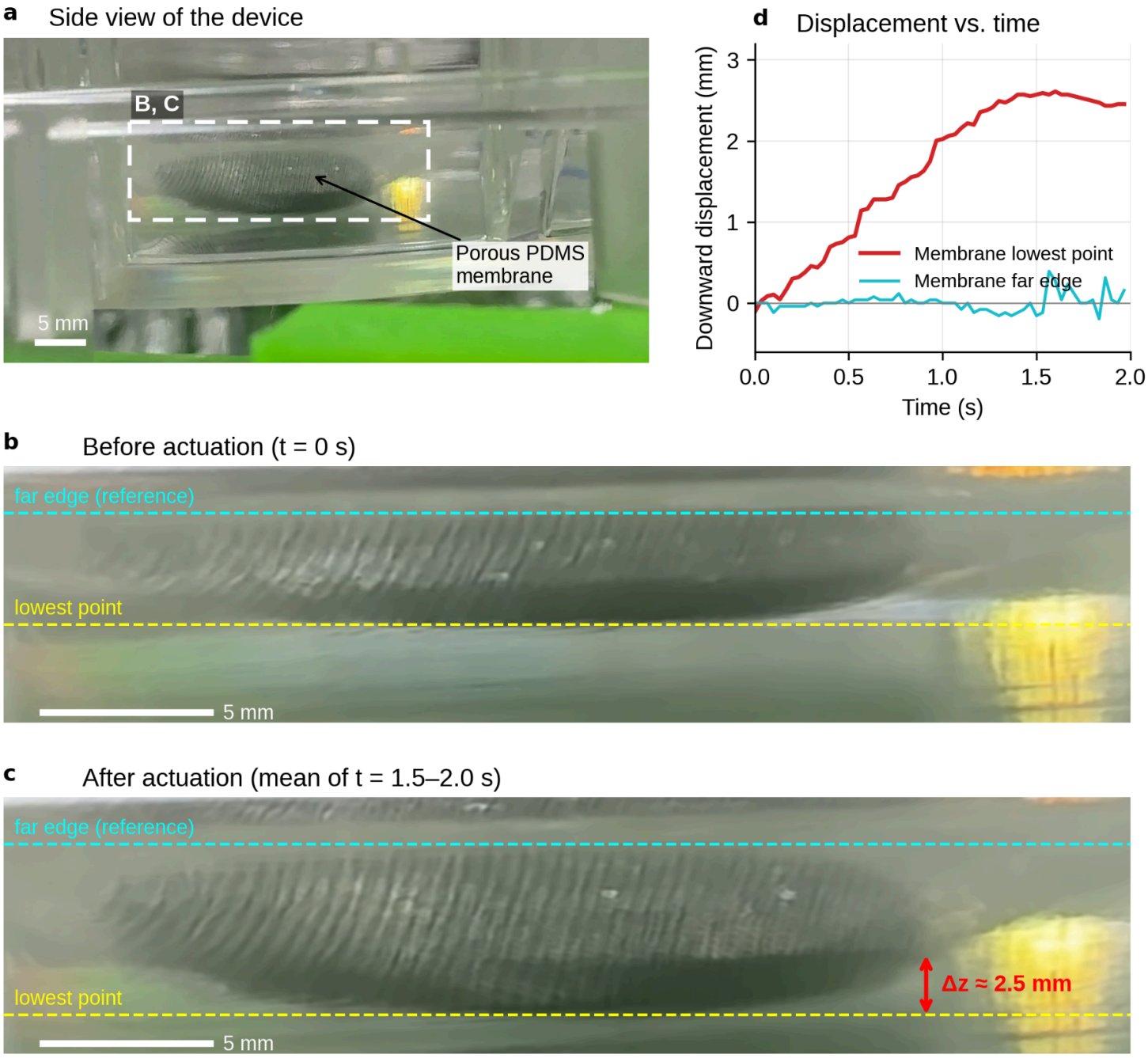


Figure 4

Representative side-view displacement measurement. (a) Side view of the 6-well device; the dashed box marks the region shown in (b,c). (b,c) Membrane before and after actuation (mean of t = 1.5–2.0 s); dashed lines mark the far edge of the membrane (cyan, fixed reference) and its lowest point (yellow). Scale bars, 5 mm in the membrane plane. (d) Downward displacement of the membrane lowest point and of the far-edge reference over time; the lowest point moved approximately 2.5 mm while the far edge remained within ±0.1 mm. Repeated actuation cycles are shown in Online Resource 2

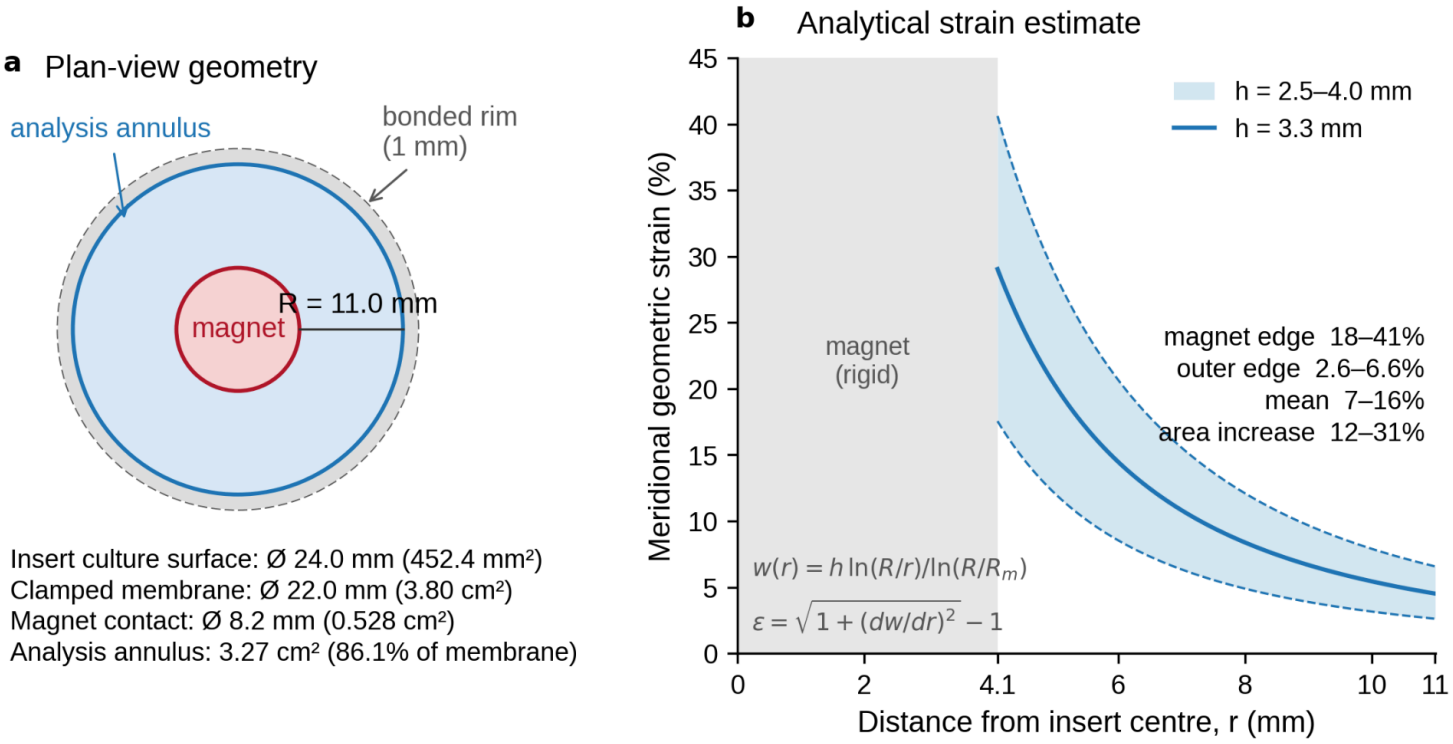


Figure 5

Plan-view geometry and analytical sensitivity estimate of membrane deformation. (a) Free membrane radius R = 11.0 mm after excluding the bonded rim; magnet contact radius Rm = 4.10 mm. (b) Geometry-based meridional strain estimate for h = 2.5–4.0 mm, with h = 3.3 mm shown as the intermediate case. This analysis is not a direct strain measurement

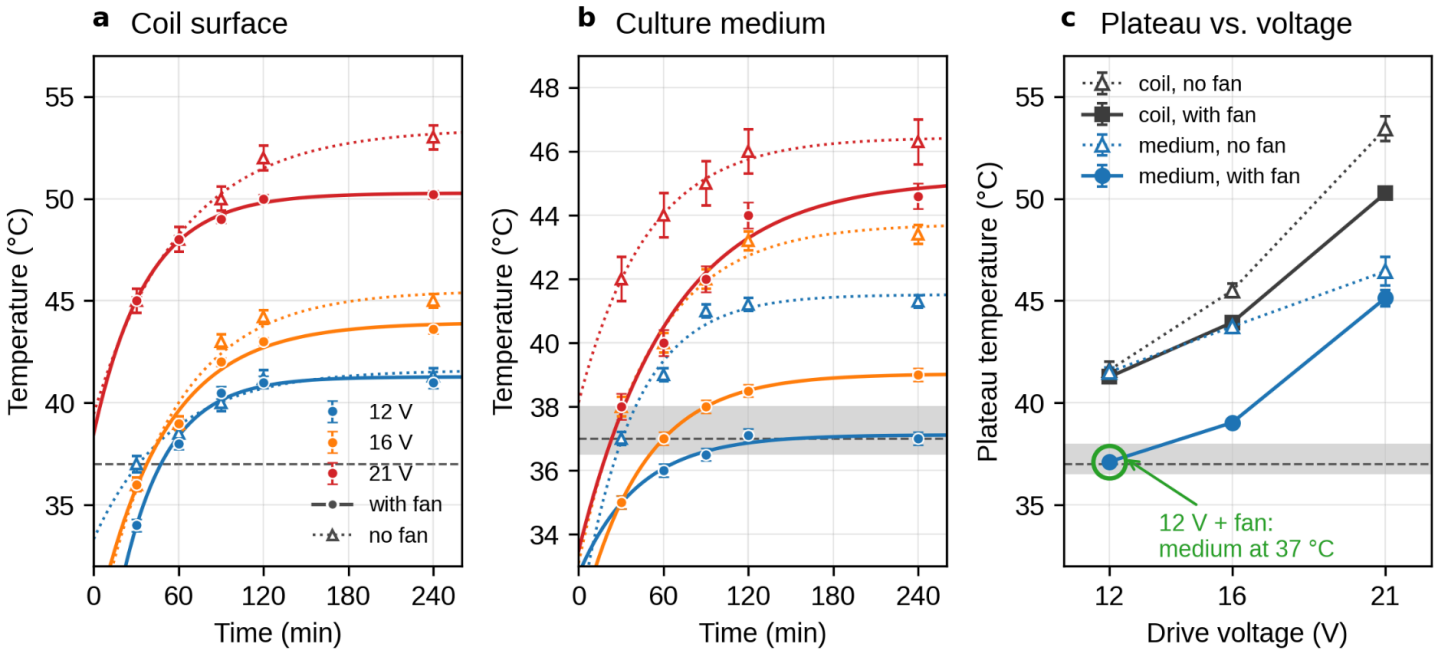


Figure 6

Thermal characterization of the magnetic actuator. (a) Coil-surface temperature and (b) culture-medium temperature during 240 min of operation at 12, 16, and 21 V with and without auxiliary fan cooling. (c) Plateau temperature versus drive voltage. The 12 V + fan condition maintained the culture medium near 37 °C and was used for dynamic culture. Error bars indicate SD

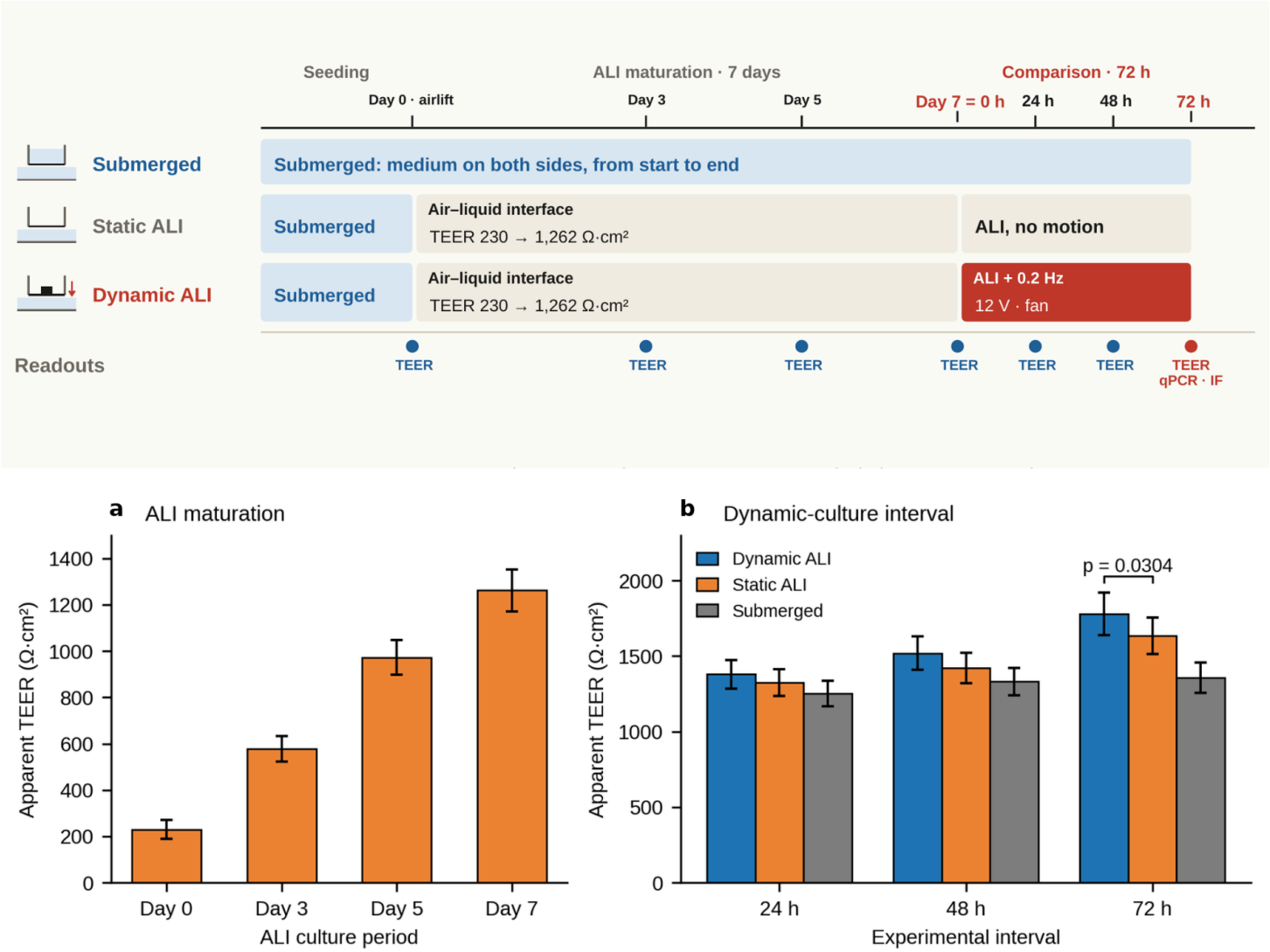


Figure 7

Experimental timeline and apparent barrier function. Top: all groups were initially seeded under submerged conditions; static-ALI and dynamic-ALI groups were air-lifted and matured for 7 days before the 72 h comparison. Dynamic ALI was operated at 0.2 Hz and 12 V with continuous fan cooling. Bottom: (a) ALI maturation (n = 9 independent inserts). (b) Experimental phase displayed in the order submerged, static ALI, and dynamic ALI at 24, 48, and 72 h (n = 9 per condition). At 72 h, dynamic ALI was higher than static ALI (two-sided independent-samples t test, p = 0.0304). Bars show mean ± SD

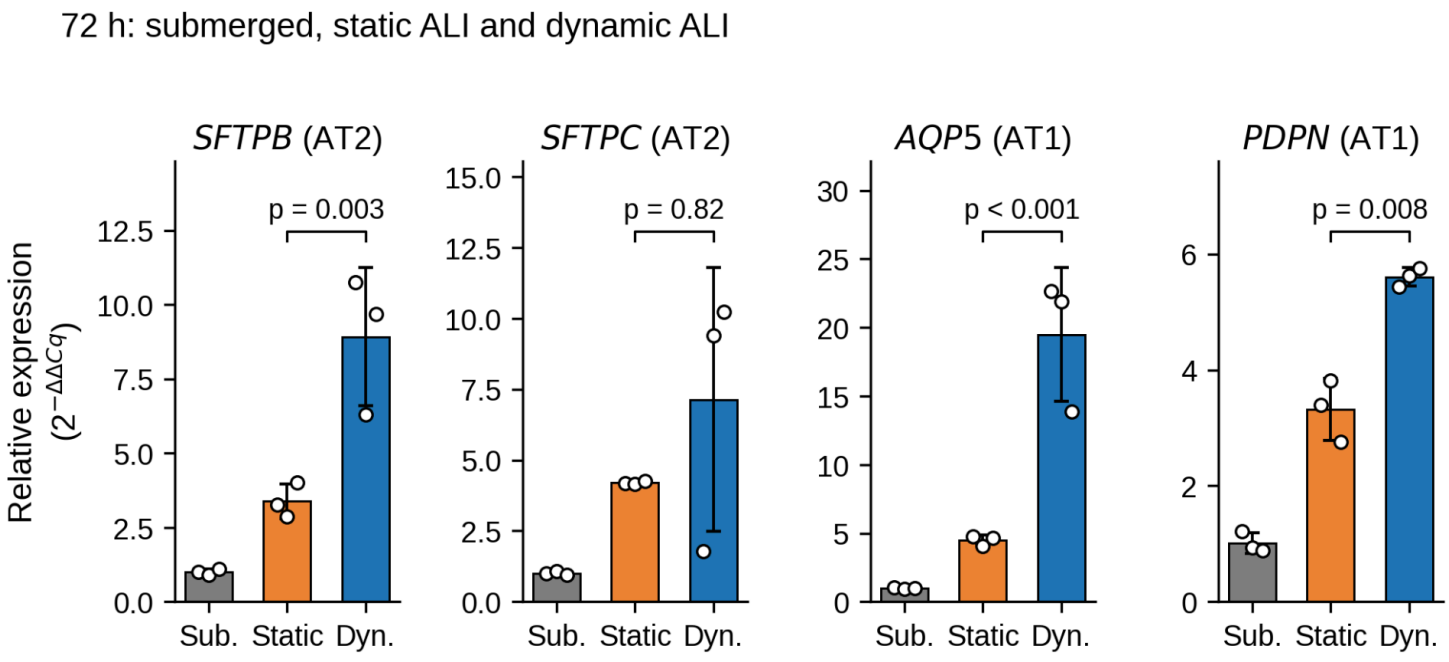


Figure 8

RT-qPCR analysis of alveolar epithelial markers at the matched 72 h endpoint. Submerged, static ALI, and dynamic ALI cultures are shown for the AT2-associated markers SFTPB and SFTPC and the AT1-associated markers AQP5 and PDPN, relative to GAPDH and to submerged culture (2^−ΔΔCq). Bars show mean ± SD and circles indicate independent inserts (n = 3); p values compare static and dynamic ALI (one-way ANOVA with Tukey HSD on ΔCq)

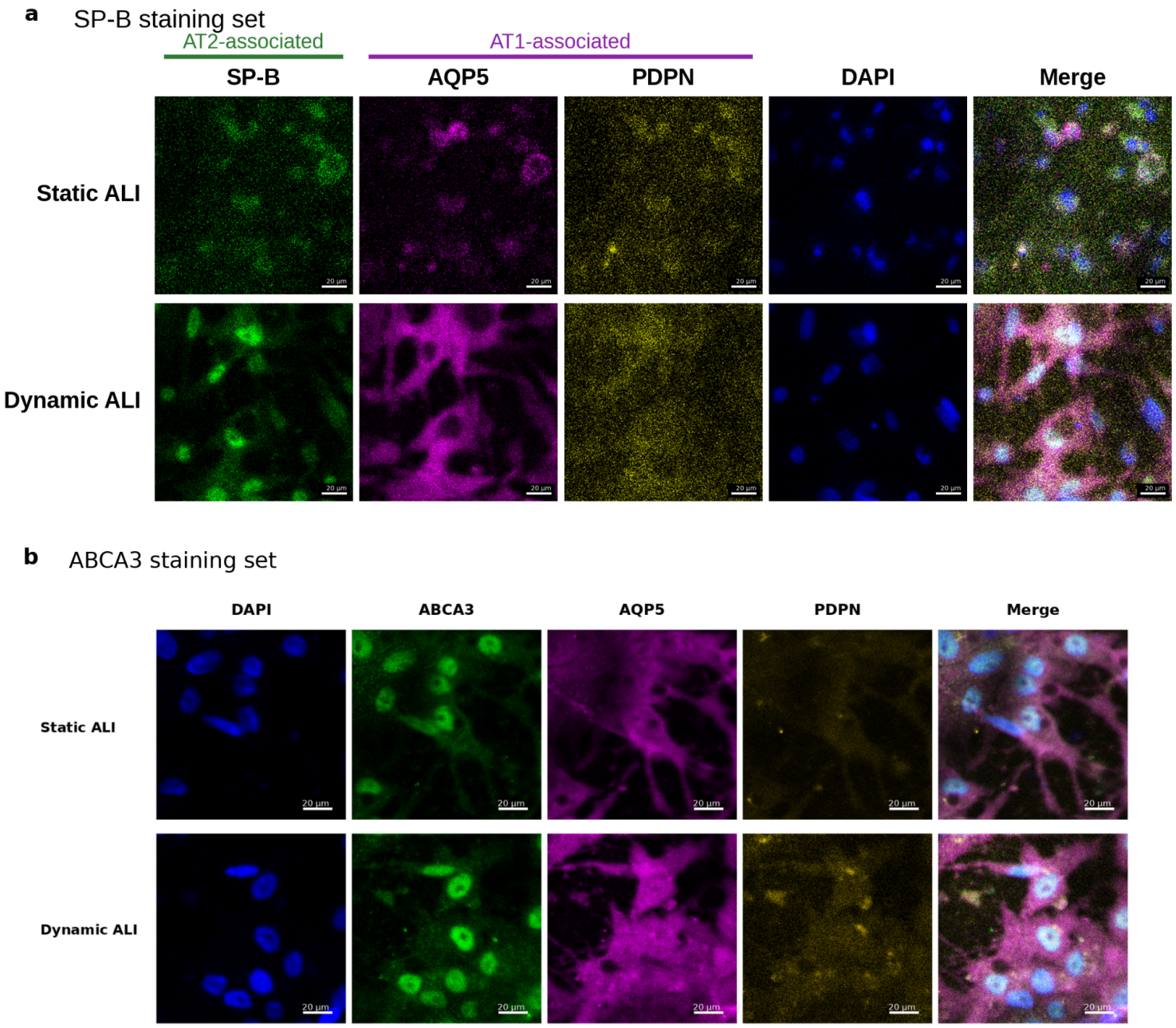


Figure 9

Whole-mount immunofluorescence of alveolar-associated markers. (a) SP-B staining set and (b) ABCA3 staining set. Within each block, rows show static and dynamic ALI. Columns are labeled in the figure and include the AT2-associated marker (SP-B or ABCA3), the AT1-associated markers AQP5 and PDPN, nuclei (DAPI), and merged fluorescence. All displayed fields use 20 μm scale bars. Images are interpreted qualitatively because acquisition settings were not fully harmonized

Supplementary Files

This is a list of supplementary files associated with this preprint. Click to download.

- LinMagneticALISupplementaryv19.docx